Directional interacting whispering-gallery modes in coupled dielectric microdisks

Jung-Wan Ryu,[1,2] Soo-Young Lee,[1] Chil-Min Kim,[1] and Young-Jai Park[2]
[1]*National Creative Research Initiative Center for Controlling Optical Chaos, Pai-Chai University, Daejeon 302-735, Korea*
[2]*Department of Physics, Sogang University, Seoul 121-742, Korea*
(Received 7 December 2005; published 17 July 2006)

We study the optical interaction in a coupled dielectric microdisks by investigating the splitting of resonance positions of interacting whispering-gallery modes (WGM's) and their pattern change, depending on the distance between the microdisks. It is shown that the interaction between the WGM's with odd parity about the y axis becomes appreciable at a distance less than a wavelength and causes directional emissions of the resulting interacting WGM's. The directionality of the interacting WGM's can be understood in terms of an effective boundary deformation in ray dynamical analysis. We also discuss the oscillation of the splitting when the distance is greater than a wavelength.

DOI: 10.1103/PhysRevA.74.013804 PACS number(s): 42.55.Sa, 42.65.Sf

I. INTRODUCTION

In spherical and cylindrical dielectric cavities high-Q modes are the whispering-gallery modes (WGM's) in which light rays circulate along the curved inner boundary of the cavities, reflecting from the boundary with an incident angle always greater than the critical angle for total internal reflection, thus remaining trapped inside the cavities [1,2]. There are only minute isotropic emissions of light caused by evanescent leakage. For the applications to optical communication and optoelectric circuit, this isotropic emission is not desirable; rather, directional emission is much more useful and effective [2].

As a simple system for directional emissions, slightly deformed microcavities have been proposed, and directional emissions, tangential from the boundary points with the highest curvature, are achieved. From the ray dynamical viewpoint, as being slightly deformed, some invariant tori are destroyed in the Poincaré surface of section (PSOS), but the Kolmogorov-Arnold-Moser (KAM) tori still confine the rays supporting the WGM's. In this case, the tunneling process, through the lowest dynamical barrier, to the critical line for the total internal reflection can explain the tangential emissions [2,3].

When the cavity boundary is highly deformed, the PSOS shows a global chaotic sea with very small integrable regions (islands). In this strong-chaotic case, the directional emissions can be found in scarred resonances [4] and quasiscarred resonances [5]. Unlike the slightly deformed case, the direction of emission in these resonances can deviate from the tangential and is well explained by the unstable manifold structure near the critical line for total internal reflection [6] and the Fresnel filtering effect [7]. In addition, there are special boundary shapes for generating unidirectional emission, spiral shaped [8] and rounded triangle shaped [9]. We note that the efforts for directional emissions are mainly based on the deformation of boundary shapes.

In this paper we show, through a numerical study of the interacting WGM's in a coupled identical disks, that a mode-mode interaction can generate directional emissions. The interaction between two WGM's is parameterized by the distance between two disks, and it turns out that the strength of the interaction between WGM's with odd parity about the y axis becomes appreciable at a distance less than a wavelength, which is evident from the results on the variation of resonance positions and patterns. In order to explain the resulting directional emission, we assume that the circular boundary shapes would be effectively deformed due to the mode-mode interaction. With this assumption the ray dynamical analysis gives a good explanation for the degradation of the Q factor and the enhancement of directional emissions. In addition, when the WGM's are weakly coupled, the resonance positions show an oscillating behavior depending on the distance.

The paper is organized as follows. In Sec. II we illustrate our system—i.e., a coupled dielectric microdisk. The numerical results for the strongly interacting WGM's and a ray dynamical model with an effective deformation are presented in Sec. III. The behavior of weakly interacting WGM's is discussed in Sec. IV. Finally, we summarize the results in Sec. V.

II. COUPLED DIELECTRIC MICRODISKS

As a simple system for the study of interacting WGM's, we take coupled dielectric microdisks. In this system, the strength of the interaction can be controlled by adjusting the distance between two disks. It is well known that the WGM's of a single dielectric microdisk are twofold degenerate due to the circular symmetry and are classified by the angular momentum mode index m and the radial mode index l [2]. Therefore, in the coupled microdisks, the WGM's would show an approximate fourfold degeneracy when the distance d between the disks is very large or, equivalently, when the interaction between WGM's is negligible. As the distance is getting smaller, the WGM in one microdisk starts to know the existence of the WGM in the other microdisk; then, the system is no longer circular symmetric, and the four fold-degenerate resonance positions start to split each other or deviate from that of the unperturbed microdisk, and the degree of the splitting measures the strength of the interaction between the WGM's.

Figure 1 shows the four symmetry classes of coupled dielectric microdisks. The system has two symmetry lines, and

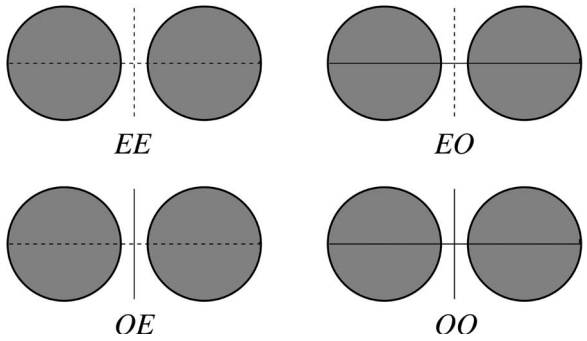

FIG. 1. The four symmetry classes of the coupled identical disks. The former letter indicates the parity on x, and the latter does the parity on y coordinates. Even (odd) symmetry is marked by dashed (solid) lines.

the former letter E (O) is even (odd) if the wave function is even (odd) with respect to $x \rightarrow -x$ and the latter refers to $y \rightarrow -y$.

In practical calculation of the interacting WGM's in the coupled dielectric microdisks, we use the boundary element method (BEM) to solve the Helmholtz equation,

$$[\nabla^2 + n^2(\mathbf{r})k^2]\psi = 0, \tag{1}$$

where $n(\mathbf{r})$ is the refractive index and k is the wave number. It is known that the BEM is effective when the boundary is strongly deformed from a circular shape and the cavities are coupled [10]. In this paper, we focus on the TM polarization where both the wave function and its normal derivative are continuous across the boundary. The radius of the disks is R, the distance between two dielectric disks is d, and n_{in} and n_{out} are the refractive indices inside and outside the disks, respectively. We set $n_{out}=1$ throughout the paper.

III. STRONGLY INTERACTING WGM's

In this section we present numerical results on the variation of resonance positions and patterns of the strongly interacting WGM's—i.e., the case of the short distance $d<\lambda$. As mentioned before, we expect that the four fold-degenerate WGM's would start to split each other due to the interaction between WGM's as the distance d decreases. As a result of the interaction the directional emissions appear in the interacting WGM's with odd parity about the y axis. We explain this directionality by assuming an effective deformation of the boundary in ray dynamical analysis. In the practical BEM calculation, we take 12 elements per a wavelength inside ($\lambda_{in}=2\pi/n_{in}k$).

A. Variation of resonance positions and patterns

Numerical calculation is performed for the WGM of mode index $(m,l)=(77,1)$ with $n_{in}=1.4$. Exact resonance positions of the WGM in an isolated microdisk can be obtained from the matching conditions between the Bessel function and the Hankel function of the first kind which are inner and outer radial solutions of the Helmholtz equation, respectively. The exact resonance position of $\mathrm{WGM}_{(77,1)}$ is kR $=59.7136-i2.5687\times10^{-8}$ where k is the vacuum wave number. The very small value of $|\mathrm{Im}(kR)|$ means high-Q factors from the relation $Q=-\mathrm{Re}[kR]/2\,\mathrm{Im}[kR]$. Unfortunately, it is very difficult to get the exact imaginary values from the BEM; for example, when we take 12 elements per λ_{in}, the BEM calculation for the isolated microdisk gives kR $=59.7155-i3.9\times10^{-3}$ for $\mathrm{WGM}_{(77,1)}$. In spite of the restriction on the precision of resonance positions, we rely on the BEM calculation in analyzing the interacting WGM's based on the following reasons. First, the change of $\delta(kR)\simeq10^{-3}$ does not give any visible variation in resonance patterns. Second, the BEM calculation would give a correct result when the variation of resonance positions exceeds the precision limit $\delta(kR)\simeq10^{-3}$.

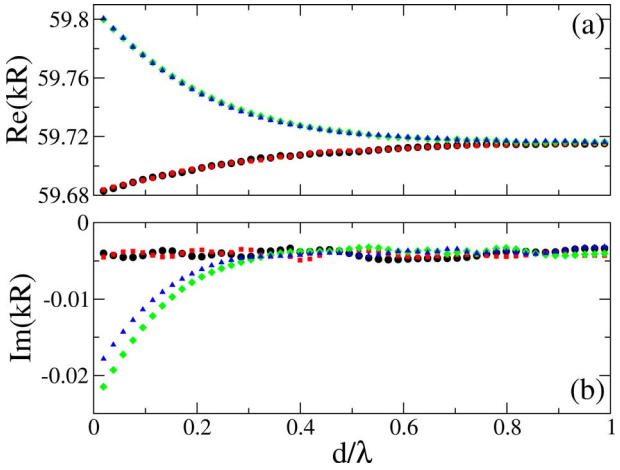

FIG. 2. (Color online) The splitting of the degenerate $\mathrm{WGM}_{(77,1)}$ due to the mode-mode interaction in the coupled disks system. $\mathrm{Re}(kR)$ (a) and $\mathrm{Im}(kR)$ (b) are plotted depending on the distance d between two disks. Note that kR converges into the resonance position of the single-disk case, $59.7155-i0.0039$ as d increases. Black circle, red square, green diamond, and blue triangle correspond to *EE*, *EO*, *OE*, and *OO* modes, respectively.

Figure 2 shows the variation of resonance positions of the interacting WGM's. The fourfold-degenerate state starts to split into two groups at $d\simeq0.8\lambda$ in $\mathrm{Re}[kR]$ and at $d\simeq0.4\lambda$ in $\mathrm{Im}[kR]$. Here we can see that the resonances with odd parity about the y axis (*OE* and *OO* modes) show larger variations, indicating that the WGM's in the resonances are strongly coupled. We note that the $\mathrm{Re}[kR]$ values of *OE* and *OO* modes increase with decreasing d. The increment of $\mathrm{Re}[kR]$ implies a reduction of the effective boundary perimeter, and the interaction between WGM's in the *OE* and *OO* modes is, thus, repulsive. From the same argument, we conclude that the interaction in the *EE* and *EO* modes is weakly attractive. This result will be used in determining the effective deformation in the ray model in the next subsection. As shown in Fig. 2(b) the $\mathrm{Im}[kR]$ values of *OE* and *OO* modes decrease with decreasing d, implying a degradation of the Q factor due to the repulsive interaction. Therefore, we can expect that the emission of the *OE* and *OO* modes would be stronger than those of the *EE* and *EO* modes. From the viewpoint of the effective boundary deformation due to the repulsive interaction, we can understand the difference of the onset

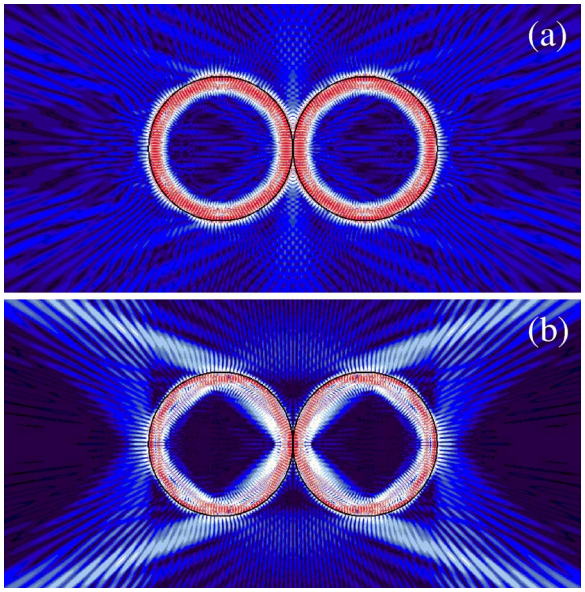

FIG. 3. (Color online) Resonance patterns of the interacting $WGM_{(77,1)}$'s when $n_{in}=1.4$ and $d=0.02\lambda$. (a) *EE* mode. (b) *OE* mode. Red-white-blue-dark blue colors indicate high to low intensity on a logarithmic scale.

points of the splitting in Re$[kR]$ and Im$[kR]$. In a slightly deformed cavity, the rays supporting the WGM are completely confined by the KAM tori, resulting in no drastic reduction of the Q factor. As the cavity is more deformed, the KAM tori would be broken and the rays can diffusively escape along the unstable manifolds, and then the Q factor, equivalently Im$[kR]$, would decrease rapidly.

From the splitting behavior of the resonance positions, we can expect that the resonance patterns of *EE* and *EO* modes would be different from those of *OE* and *OO* modes. In Fig. 3 the resonance patterns of the interacting $WGM_{(77,1)}$'s are shown when the distance d is 0.02λ. The resonance position of *EE* mode shown in Fig. 3(a) is $kR=59.6829-i0.0040$ and, as expected from the small absolute value of Im$[kR]$, the very small evanescent leakage is shown [11]. However, as shown in Fig. 3(b), the resonance pattern of the *OE* mode ($kR=59.7998-i0.0215$) shows clear directional emissions, reflecting the strong repulsive mode-mode interaction. Its far-field emission pattern is plotted in Fig. 4(a) where the four strong directional emissions are clearly seen. We find that the directionality of the emission pattern is insensitive to the distance d, although the strength of emissions decreases with increasing d.

In the *OE* and *OO* modes, the strong directional emission by the repulsive mode-mode interaction is a generic feature, but the emission directions are closely related to the reflective index n_{in}. As an example, the resonance patterns of the *EE* and *OE* modes in the interacting $WGM_{(29,1)}$'s, when $n_{in}=2.0$ and $d=0.005\lambda$, are shown in Fig. 5. As expected, four strong directional emissions are shown only in the *OE* resonance pattern in Fig. 5(b), and the two beams emitted from one disk are almost parallel to the x axis. Note that the direction of emission is quite different from that of the interacting $WGM_{(77,1)}$ in Fig. 3(b). The corresponding far-field

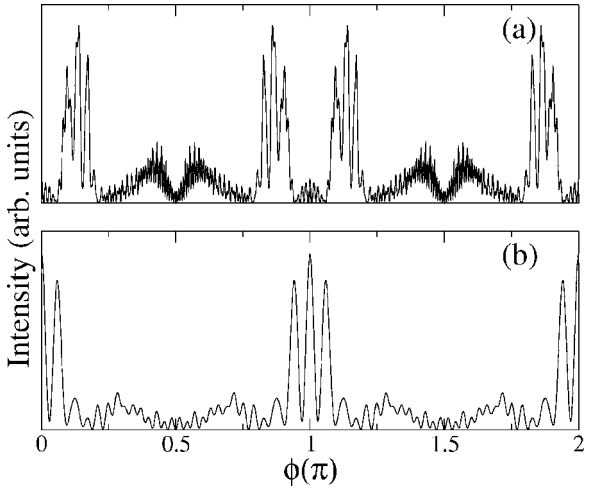

FIG. 4. The far-field emission patterns of the interacting WGM's. (a) The interacting $WGM_{(77,1)}$'s ($n_{in}=1.4$) shown in Fig. 3(b). (b) The interacting $WGM_{(29,1)}$'s ($n_{in}=2.0$) shown in Fig. 5(b).

emission pattern is shown in Fig. 4(b) where we confirm the two directional emissions along the x axis and clear interference pattern of the parallel beams.

In the next subsection we will introduce a ray dynamical model to explain the n_{in} dependence of the directionality of emissions in the interacting WGM's with *OE* and *OO* parities.

B. Ray dynamical model: Effective deformation

In a circular disk, the ray dynamics is simple. The rays with incident angles greater than the critical angle, $\theta_c=\arcsin(1/n_{in})$, are perfectly confined in the disk by the total

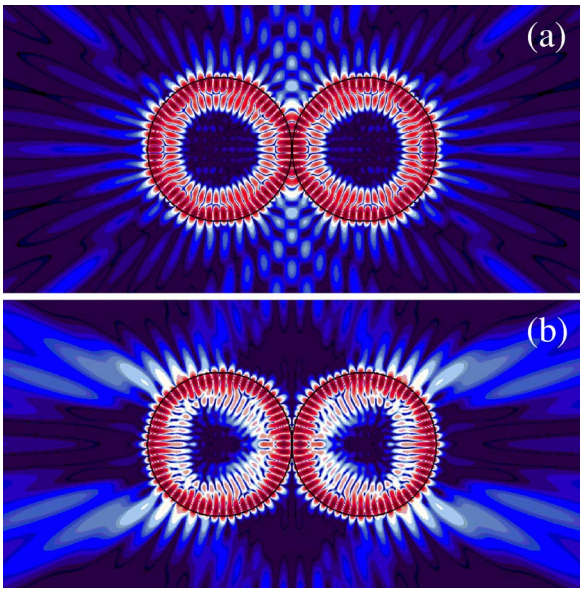

FIG. 5. (Color online) Resonance patterns of the interacting $WGM_{(29,1)}$'s when $n_{in}=2.0$ and $d=0.005\lambda$. (a) *EE* mode. (b) *OE* mode. Red-white-blue-dark blue colors indicate high to low intensity on a logarithmic scale.

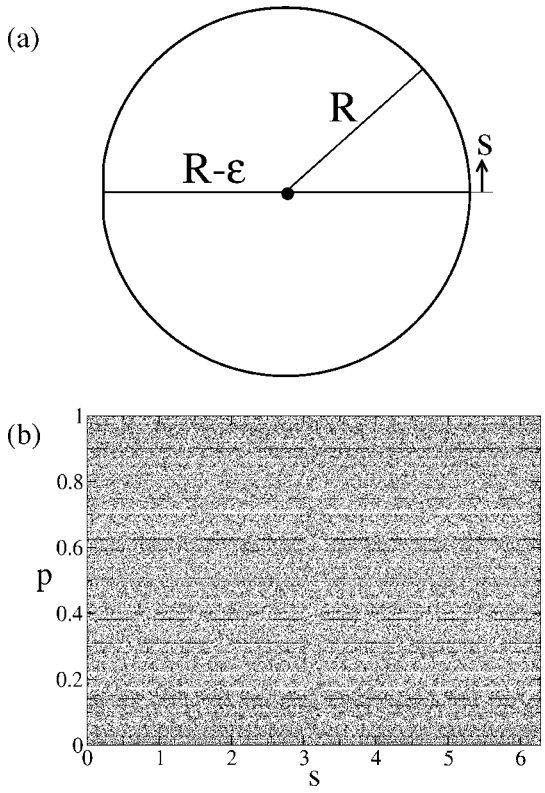

FIG. 6. (a) The boundary shape used in the ray dynamical analysis, a circle with a cut. (b) PSOS for the billiard shown in (a) when $R=1$ and $\epsilon=0.01$.

internal reflection, while the other rays escape isotropically due to its rotational symmetry. With a simple combination of this trivial ray dynamics, it is impossible to explain the directionality of the interacting WGM's shown in the previous subsection.

We recall that the interaction between WGM's are repulsive in the *OE* and *OO* modes. In fact, this originates from the constraint that the field value at $x=0$ or on the y axis should be zero due to the odd parity about the y axis. As a result, the intensity spots confronting each other near $x=0$ would shift repulsively and the structure of the whole intensity spots in a WGM would be slightly deformed from a circle. In order to incorporate this effect of the repulsive interaction into the ray dynamics, we consider a slightly deformed circular boundary which can support the slightly deformed WGM similar to one of the interacting WGM's.

As a simple ray dynamical model containing the effect of the repulsive interaction, we consider a circular disk with a cut as shown in Fig. 6(a). The deformation parameter is ϵ which is the reduced length of the radius by the cut. Figure 6(b) shows its PSOS representing the trajectory of a ray starting from one point in phase space (s,p), where s is the boundary coordinate and $p=\sin\theta$, θ being the incident angle, without consideration of the refractive escape. Since the circle with a cut is a discontinuous deformation (non-KAM system), this model cannot describe the weakly deformed case where the rays supporting the WGM are still confined in KAM tori. So our model is more suitable to a moderately deformed case where the rays supporting the WGM can diffusively escape. The rays can change their incident angle only through the bounce on the cut, and eventually the ray trajectory fills up the whole phase space, even though there are so many marginally stable lines. The broken lines at $p\sim0.50$ and $p\sim0.71$ represent the families of the marginally stable triangular and rectangular periodic orbits, and the gaps of lines correspond to the cut of the boundary.

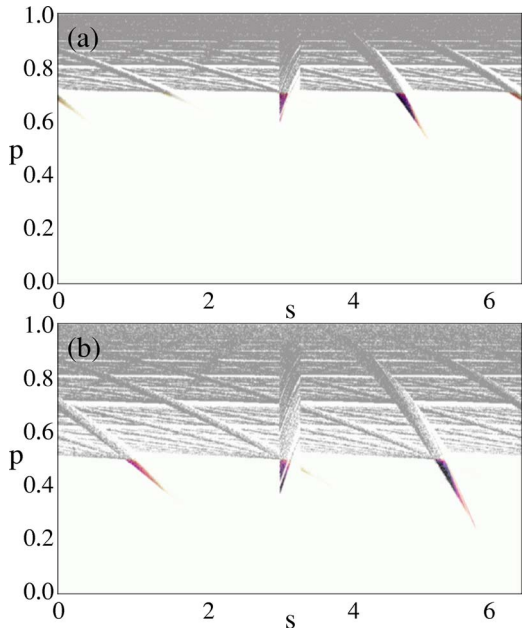

FIG. 7. (Color online) The survival probability distribution. The colored spikes show the parts through which long-lived rays escape. (a) $n_{in}=1.4$ case. (b) $n_{in}=2.0$ case.

The dielectric microcavities are open systems where rays can refractively escape from the microcavities, and the escape rates are determined by the Fresnel equations [12]. In order to understand the emission direction of rays, we obtain the survival probability distributions in both cases of $n_{in}=1.4$ and $n_{in}=2.0$ which are shown in Figs. 7(a) and 7(b), respectively. The gray points in Fig. 7 correspond to the rays with normalized probability greater than 0.1 in the time range of $50<t<53$ with a time scale as the length of the ray trajectory, and the rays start from a uniform ensemble of 1000×1000 initial positions in the phase space. The pattern of the survival probability distribution reveals the openness structure on the unstable manifold background near the critical lines, $p_c=1/n_{in}$, for the total internal reflection. The directionality of emissions and the emitting part of boundary are explained by the pattern below the critical line. The color plots below the critical lines in Figs. 7(a) and 7(b) illustrate how the long-lived rays supporting the WGM's can escape. We find that the long-lived rays refractively escape through the unstable manifold structure arising in the survival probability distribution. As mentioned before, the ray far above the critical line changes its angular momentum only when bouncing from the cut and, depending on the bouncing position on the cut, the angular momentum can increase or decrease; in other words, the angular momentum diffuses to other values. From repetition of this diffusion process, the ray can reach below the critical line and eventually escape

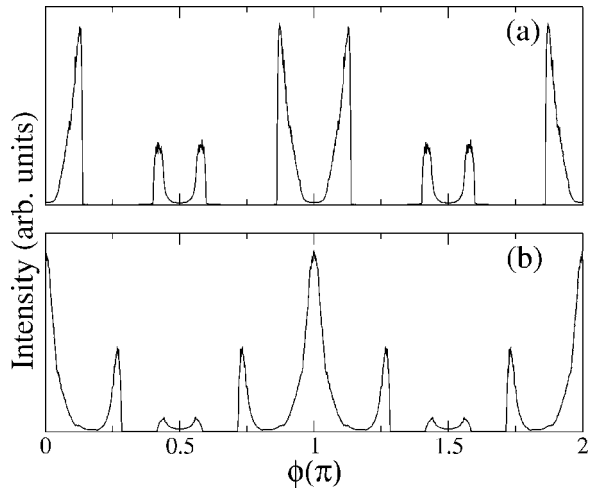

FIG. 8. The ray dynamical far-field emission patterns of the deformed dielectric disk. (a) $n_{in}=1.4$ case. (b) $n_{in}=2.0$ case.

the microcavity. The ensemble of the above escape process makes the color plots. The darkness of the color plots represents the population of the ensemble.

The colored spikes below the critical line ($p_c \simeq 0.714$) in Fig. 7(a) correspond to the rays following the diamond-type period orbit inside the microcavity and indicate that the ray emission from about $s=3\pi/2$ is very strong for the counterclockwise circulating rays ($p>0$). These are consistent with the resonance pattern shown in Fig. 3(b) where the faint diamond structure is seen inside the microdisks and the strong emission comes out from about $s=3\pi/2$ of the right microdisk. If we consider another effective deformed microcavity to simulate the interacting WGM's, we can get the resulting emission pattern shown in Fig. 8(a) where we neglect the emission from the cut. This ray dynamical result is very similar to the far field emission pattern of Fig. 4(a) except the interference oscillation in peaks. The same discussion is valid for the case of $n_{in}=2$ case shown in Fig. 7(b). The resulting emission pattern is given in Fig. 8(b), and this explains well the far-field pattern of the interacting WGM's shown in Fig. 4(b).

Although the deformed disk in Fig. 6(a) is a non-KAM system, this explains well the insensibility of the directionality of emissions to the distance d. The longer distance d corresponds to the smaller ϵ value. In this case, although the average escape rate and the emitting part of the boundary would decrease, it is clear that the emission directions and the emitting positions on the boundary are essentially invariant. However, the mode-mode interaction would create a continuous deformation; i.e., the system would be a KAM system. In a KAM model, even if the rays supporting the WGM are confined in KAM tori, it is still possible for the rays to reach chaotic sea through the dynamical tunneling and then diffuse along the unstable manifolds to the critical line [13]. The unstable manifold structure near the critical line in the KAM model would be similar to that of the non-KAM model if the global boundary shapes of both models are almost identical. Therefore, both models would give the essentially same emission directionality.

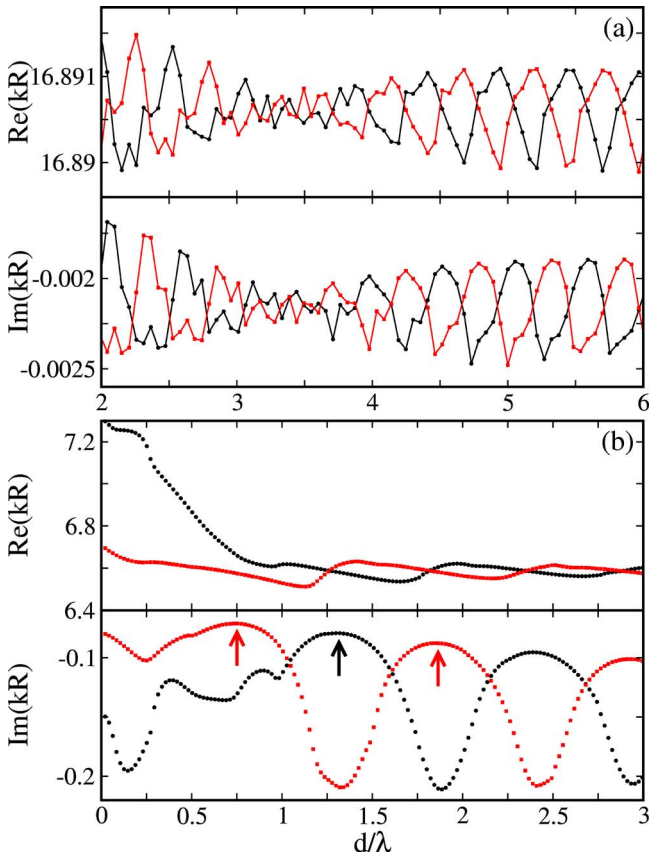

FIG. 9. (Color online) The oscillatory behavior of the resonance position of interacting WGM's when $d>\lambda$. (a) $\mathrm{WGM}_{(29,1)}$ case. (b) $\mathrm{WGM}_{(7,2)}$ case. The black circle and red square denote *EE* and *OE* modes, respectively.

IV. WEAKLY INTERACTING WGM's

When the distance d is larger than λ, the interaction between WGM's becomes very small. The strength of the small interaction can be measured by the deviation of resonance position from that of isolated corresponding WGM as done for the strongly interacting WGM's in the previous section. Figure 9(a) shows the variation of the resonance position in the range of $2\lambda<d<6\lambda$ for the interacting $\mathrm{WGM}_{(29,1)}$'s with $n_{in}=2$. It is shown that the resonance positions of both *EE* (black circle) and *OE* (red square) modes oscillate with the period $\Delta d \simeq \lambda/2$. The oscillatory behavior also appears for *EO* and *OO* modes. The interference effect of emitted waves from the WGM's seems to be responsible for the oscillatory behavior. As pointed out in the previous section, the BEM calculation, however, has the precision limit of $\delta(kR) \simeq 10^{-3}$. We note that the amplitude of the oscillations is almost the same order as the precision limit. So we have to be careful to accept the oscillatory behavior as a real phenomenon, because it can be a numerical artifact. To check this, we performed the same calculation for the interacting $\mathrm{WGM}_{(7,2)}$'s ($n_{in}=2.0$) which are relatively low-Q resonance modes. Since the emission of the $\mathrm{WGM}_{(7,2)}$ is stronger than the $\mathrm{WGM}_{(29,1)}$ case, we expect the variation of the resonance position would be larger than the precision of BEM.

The exact resonance position of the $WGM_{(7,2)}$ in an isolated circular disk is $kR=6.5806-i0.1117$ and, in the BEM, $kR=6.5808-i0.1127$, giving the same precision limit of $\delta(kR)\simeq 10^{-3}$. For the interacting $WGM_{(7,2)}$'s, the variations of resonance positions for *EE* and *OE* modes are shown in Fig. 9(b). When $d\gtrsim\lambda$, both real and imaginary parts of kR oscillate with a period $\Delta d\simeq\lambda$ and the oscillation amplitude is much greater than the precision limit of the BEM, which supports the conjecture that the oscillatory behavior of the interacting $WGM_{(29,1)}$ in Fig. 9(a) would be a real phenomenon, not a numerical artifact. We note that the oscillation of the resonance position of the *OE* mode is out of phase with that of the *EE* mode in both $\mathrm{Re}(kR)$ and $\mathrm{Im}(kR)$. The resonance patterns at the local maxima of $\mathrm{Im}(kR)$, corresponding to minimum leakages of the system, denoted by arrows in Fig. 9(b), are shown in Fig. 10, and these explain why the oscillations of the resonance positions of *OE* and *EE* modes are out of phase and have a period $\Delta d\simeq\lambda$. The internal patterns of the resonances are almost invariant, and the characteristic difference is the number of intensity spots on the horizontal axis between two disks which increases one by one. An odd and even number of spots appear in the *OE* and *EE* modes, respectively. Roughly we can understand this oscillation behavior as the degree of the accordance with the quantization condition of the unstable periodic orbit lying on the horizontal axis between two disks even though the boundary condition on the ends of the period orbit is not trivial. In fact this kind of explanation is valid only for the relatively low-kR case where the interference on the unstable orbit dominates and other inference effects are negligible. In the high-kR case many beams emitted from the intensity spots inside the disks take part in the interference process, and the resulting oscillation of each symmetry mode would show more complicated behavior in its period and amplitude.

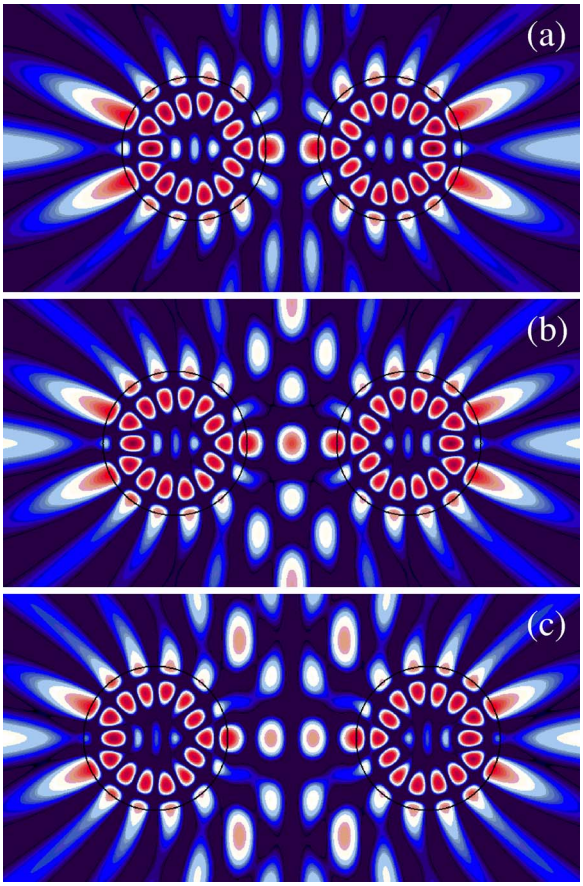

FIG. 10. (Color online) Resonance patterns of those corresponding to the maxima of the oscillation indicated by arrows in Fig. 9(b). The resonance positions are (a) $kR=6.5744-i0.0712$ (*OE* mode), (b) $kR=6.5824-i0.0793$ (*EE* mode), and (c) $kR=6.5812-i0.0877$ (*OE* mode). $n_{in}=2.0$ is used, and red-white-blue-dark blue colors indicate high to low intensity on a logarithmic scale.

V. SUMMARY

In the coupled-disk system, we have shown that the strongly interacting WGM's with odd parity about the y axis give good directional emissions and the directions of the emissions are determined by the refractive index of the dielectric disks. This finding has been well explained by an effective boundary deformation in the ray dynamical model. It is also shown that the resonance positions of the weakly interacting WGM's oscillate depending on the distance d between two microdisks and this oscillation can be understood as the result of interference of emitted beams from the WGM's.

ACKNOWLEDGMENT

This work is supported by Creative Research Initiatives of the Korean Ministry of Science and Technology.

[1] S. L. McCall, A. F. J. Levi, R. E. Slusher, S. J. Pearton, and R. A. Logan, Appl. Phys. Lett. **60**, 20 (1992); Y. Yamamoto and R. E. Slusher, Phys. Today **46**(6), 66 (1993).

[2] *Optical Processes in Microcavities*, edited by R. K. Chang and A. J. Campillo (World Scientific, Singapore, 1996).

[3] A. Mekis, J. U. Nöckel, G. Chen, A. D. Stone, and R. K. Chang, Phys. Rev. Lett. **75**, 2682 (1995); J. U. Nöckel, A. D. Stone, G. Chen, H. L. Grossman, and R. K. Chang, Opt. Lett. **21**, 1609 (1996); J. U. Nöckel and A. D. Stone, Nature (London) **385**, 45 (1997).

[4] E. J. Heller, Phys. Rev. Lett. **53**, 1515 (1984); S.-B. Lee, J.-H. Lee, J.-S. Chang, H.-J. Moon, S. W. Kim, and K. An, *ibid.* **88**, 033903 (2002); C. Gmachl, E. E. Narimanov, F. Capasso, J. N. Baillargeon, and A. Y. Cho, Opt. Lett. **27**, 824 (2002); T. Harayama, T. Fukushima, P. Davis, P. O. Vaccaro, T. Miyasaka, T. Nishimura, and T. Aida, Phys. Rev. E **67**, 015207(R) (2003).

[5] S.-Y. Lee, S. Rim, J.-W. Ryu, T.-Y. Kwon, M. Choi, and C.-M. Kim, Phys. Rev. Lett. **93**, 164102 (2004).

[6] H. G. L. Schwefel, N. B. Rex, H. E. Tureci, R. K. Chang, A.

D. Stone, T. Ben-Messaoud, and J. Zyss, J. Opt. Soc. Am. B **21**, 923 (2004); S.-Y. Lee, J.-W. Ryu, T.-Y. Kwon, S. Rim, and C.-M. Kim, Phys. Rev. A **72**, 061801(R) (2005).

[7] N. B. Rex, H. E. Tureci, H. G. L. Schwefel, R. K. Chang, and A. D. Stone, Phys. Rev. Lett. **88**, 094102 (2002).

[8] G. D. Chern, H. E. Tureci, A. D. Stone, R. K. Chang, M. Kneissl, and N. M. Johnson, Appl. Phys. Lett. **83**, 1710 (2003); M. Kneissl, M. Teepe, N. Miyashita, N. M. Johnson, G. D. Chern, and R. K. Chang, *ibid.* **84**, 2485 (2004); T. Ben-Messaoud and J. Zyss, *ibid.* **86**, 241110 (2005).

[9] M. S. Kurdoglyan, S.-Y. Lee, S. Rim, and C.-M. Kim, Opt. Lett. **29**, 2758 (2004).

[10] J. Wiersig, J. Opt. A, Pure Appl. Opt. **5**, 53 (2003); S.-Y. Lee, M. S. Kurdoglyan, S. Rim, and C.-M. Kim, Phys. Rev. A **70**, 023809 (2004).

[11] The intensity outside disks of Fig. 3(a) is much smaller than that of Fig. 3(b) but for convenient sake, we show the near-field intensity patterns with different intensity scale. It is the same as Fig. 5.

[12] J. F. B. Hawkes and I. D. Latimer, *Lasers: Theory and Practice* (Prentice-Hall, Englewood Cliffs, NJ, 1995).

[13] V. A. Podolskiy and E. E. Narimanov, Opt. Lett. **30**, 474 (2005).